

# Gaia Data Release 2

## Variable stars in the colour-absolute magnitude diagram

Gaia Collaboration, L. Eyer<sup>1</sup>, L. Rimoldini<sup>2</sup>, M. Audard<sup>1,2</sup>, R.I. Anderson<sup>3,1</sup>, K. Nienartowicz<sup>4</sup>, F. Glass<sup>2</sup>, O. Marchal<sup>2,5</sup>, M. Grenon<sup>1</sup>, N. Mowlavi<sup>1,2</sup>, B. Holl<sup>1,2</sup>, G. Clementini<sup>6</sup>, C. Aerts<sup>7,19</sup>, T. Mazeh<sup>16</sup>, D.W. Evans<sup>8</sup>, L. Szabados<sup>23</sup>, and 438 co-authors

(Affiliations can be found after the references)

Received ; accepted

### ABSTRACT

**Context.** The ESA *Gaia* mission provides a unique time-domain survey for more than 1.6 billion sources with  $G \lesssim 21$  mag.

**Aims.** We showcase stellar variability across the Galactic colour-absolute magnitude diagram (CaMD), focusing on pulsating, eruptive, and cataclysmic variables, as well as on stars exhibiting variability due to rotation and eclipses.

**Methods.** We illustrate the locations of variable star classes, variable object fractions, and typical variability amplitudes throughout the CaMD and illustrate how variability-related changes in colour and brightness induce ‘motions’ using 22 months worth of calibrated photometric, spectrophotometric, and astrometric *Gaia* data of stars with significant parallax.

To ensure a large variety of variable star classes to populate the CaMD, we crossmatch *Gaia* sources with known variable stars. We also used the statistics and variability detection modules of the *Gaia* variability pipeline. Corrections for interstellar extinction are not implemented in this article.

**Results.** *Gaia* enables the first investigation of Galactic variable star populations across the CaMD on a similar, if not larger, scale than previously done in the Magellanic Clouds. Despite observed colours not being reddening corrected, we clearly see distinct regions where variable stars occur and determine variable star fractions to within *Gaia*’s current detection thresholds. Finally, we show the most complete description of variability-induced motion within the CaMD to date.

**Conclusions.** *Gaia* enables novel insights into variability phenomena for an unprecedented number of stars, which will benefit the understanding of stellar astrophysics. The CaMD of Galactic variable stars provides crucial information on physical origins of variability in a way previously accessible only for Galactic star clusters or external galaxies. Future *Gaia* data releases will enable significant improvements over the present preview by providing longer time series, more accurate astrometry, and additional data types (time series BP and RP spectra, RVS spectra, and radial velocities), all for much larger samples of stars.

**Key words.** stars: general – Stars: variables: general – Stars: oscillations – binaries: eclipsing – Surveys – Methods: data analysis

### 1. Introduction

The ESA space mission *Gaia* (Gaia Collaboration et al. 2016b) has been conducting a unique survey since the beginning of its operations (end of July 2014). Its uniqueness derives from several aspects that we list in the following paragraphs.

Firstly, *Gaia* delivers nearly simultaneous measurements in the three observational domains on which most stellar astronomical studies are based: astrometry, photometry, and spectroscopy (Gaia Collaboration et al. 2016a; van Leeuwen et al. 2017).

Secondly, the *Gaia* data releases provide accurate astrometric measurements for an unprecedented number of objects. In particular trigonometric parallaxes carry invaluable information, since they are required to infer stellar luminosities, which form the basis of the understanding of much of stellar astrophysics. Proper and orbital motions of stars further enable mass measurements in multiple stellar systems, as well as the investigation of cluster membership.

Thirdly, *Gaia* data are homogeneous across the entire sky, since they are observed with a single set of instruments and are not subject to the Earth’s atmosphere or seasons. All-sky surveys cannot be achieved using a single ground-based telescope; surveys using multiple sites and telescopes/instruments require cross-calibration, which unavoidably introduce systematics and

reduce precision via increased scatter. Thus, *Gaia* will play an important role as a standard source in cross-calibrating heterogeneous surveys and instruments, much like the *Hipparcos* mission (Perryman et al. 1997; ESA 1997) did in the past. Of course, *Gaia* represents a quantum leap from *Hipparcos* in many regards, including four orders of magnitude increase in the number of objects observed, providing additional types of observations (spectrophotometry, spectroscopy), and providing significantly improved sensitivity and precision for all types of measurements.

Fourthly, there are unprecedented synergies for calibrating distance scales using *Gaia*’s dual astrometric and time-domain capabilities (e.g. Eyer et al. 2012). Specifically, *Gaia* will enable the discovery of unrivalled numbers of standard candles residing in the Milky Way, and anchor Leavitt laws (period-luminosity relations) to trigonometric parallaxes (see Gaia Collaboration et al. 2017; Casertano et al. 2017, for two examples based on the first *Gaia* data release).

Variable stars have since long been recognized to offer crucial insights into stellar structure and evolution. Similarly, the Hertzsprung-Russell diagram (HRD) provides an overview of all stages of stellar evolution and—together with its empirical cousin, the colour-magnitude-diagram (CMD)—has shaped stellar astrophysics like no other diagram. Among the first to notice the immense potential of studying variable stars in populations,

where distance uncertainties did not introduce significant scatter, was Henrietta Leavitt (1908). Soon thereafter, Leavitt & Pickering (1912) discovered the period-luminosity relation of Cepheid variables, which has become a cornerstone of stellar physics and cosmology. It appears that Eggen (1951, his fig. 42) was the first to use (photoelectric) observations of variable stars (in this case classical Cepheids) to constrain regions where Cepheids occur in the HRD; nowadays, these regions are referred to as instability strips. Eggen further illustrated how Cepheids change their locus in the colour-absolute magnitude diagram (CaMD) during the course of their variability, thus developing a time-dependent CMD for variable stars. Kholopov (1956) and Sandage (1958) later illustrated the varying locations of variable stars in the HRD using classical Cepheids located within star clusters. Combining the different types of *Gaia* time series data with *Gaia* parallaxes, we are now in a position to construct time-dependent CaMD towards any direction in the Milky Way, building on previous work based on *Hipparcos* (Eyer et al. 1994; Eyer & Grenon 1997), but on a much larger scale.

Many variability (ground- and space-based) surveys have exploited the power of identifying variable stars in stellar populations at similar distances, e.g. in star clusters or nearby galaxies like the Magellanic Clouds. Ground-based microlensing surveys such as the Optical Gravitational Lensing Experiment (OGLE; e.g. Udalski et al. 2015), the Expérience pour la Recherche d’Objets Sombres (EROS Collaboration et al. 1999), the Massive Compact Halo Objects project (MACHO; Alcock et al. 1993) deserve a special mention in this regard. The data will continue to grow with the next large multi-epoch surveys such as the Zwicky Transient Facility (Bellm 2014) and the Large Synoptic Survey Telescope (LSST Science Collaboration et al. 2009) from ground, and the Transiting Exoplanet Survey Satellite (TESS; Ricker et al. 2015) and PLATO (Rauer et al. 2014) from space.

Another ground-breaking observational trend has been the long-term high-precision high-cadence uninterrupted space photometry with CoRoT/BRITE (Auvergne et al. 2009; Pablo et al. 2016, with time bases up to 5 months) and *Kepler*/K2 (Gilliland et al. 2010; Howell et al. 2014, with time bases up to 4 years and 3 months, respectively) provided entirely new insights into  $\mu$ mag-level variability of stars, with periodicities ranging from minutes to years. These missions opened up stellar interiors from the detection of solar-like oscillations of thousands of sun-like stars and red giants (e.g., Bedding et al. 2011; Chaplin & Miglio 2013; Hekker & Christensen-Dalsgaard 2017, for reviews), as well as hundreds of intermediate-mass stars (e.g., Aerts 2015; Bowman 2017) and compact pulsators (e.g., Hermes et al. 2017). Our results provided in Sects 3 and 4 on the variability fractions and levels are representative of mmag-level variability and not of  $\mu$ mag-levels as found in space asteroseismic data.

Still, any of these asteroseismic surveys can benefit from the *Gaia* astrometry, so that distances and luminosities can be derived, as De Ridder et al. (2016) and Huber et al. (2017) did with *Gaia* DR1 data. *Gaia* will also contribute to these surveys with its photometry and some surveys will also benefit from the *Gaia* radial velocities (depending on their operating magnitude range).

Stellar variability comprises a large variety of observable features due to different physical origins. Figure 1 shows the updated Variability Tree (Eyer & Mowlavi 2008), which provides a useful overview of the various types of variability and their known causes. The Variability Tree has four levels: the distinction of intrinsic versus extrinsic variability, the separation into major types of objects (asteroid, stars, AGN), the physical origin of the variability, and the class name. In this article, we follow the classical distinction of the different causes of the variability

phenomena: variability induced by pulsation, rotation, eruption, eclipses, and cataclysmic events. A large number of variability types can already be identified in the *Gaia* data, as described in the subsequent sections.

Herein, we provide an overview of stellar variability across the CaMD, building on the astrometric and photometric data of the second *Gaia* data release (DR2). Future *Gaia* DRs will enable much more detailed investigations of this kind using longer temporal baselines, greater number of observations, and added classes of variable stars (such as eclipsing binaries, which will be published in DR3).

This paper is structured as follows. Section 2 shows the location of different variability types in the CaMD, making use of known objects from the literature which are published in *Gaia* DR2, but without any further analysis of the *Gaia* data. Section 3 presents the fraction of variables as a function of colour and absolute magnitude, obtained by processing the *Gaia* time series for the detection of variability (Eyer et al. 2018). Section 4 investigates the variability level in the CaMD, employing statistics and classification results (some of which are related to unpublished *Gaia* time series). Section 5 shows the motion of known variable stars in the CaMD, that is, a *time-dependent CaMD*, which includes also sources not available in the DR2 archive but as online material. Section 6 summarizes and presents an outlook to future *Gaia* DRs. Further information on the literature cross-match and on the selection criteria applied to our data samples can be found in Appendices A and B, respectively.

## 2. Location of variability types in the CaMD

The precision of the location in the CaMD depends on the precision of the colour on one side, and on the determination of the absolute magnitude on the other side. The precision of the absolute magnitude of variable stars depends on the photometric precision, the number of measurements, the amplitude of variability, and the relative parallax precision  $\sigma_{\varpi}/\varpi$ . The upper limits of  $\sigma_{\varpi}/\varpi$  employed in this article vary between 5 and 20 per cent, so the uncertainty of the absolute magnitude solely due to the parallax uncertainty can be as large as  $5(\ln 10)^{-1}\sigma_{\varpi}/\varpi \approx 0.43$  mag.

As we determined the colour as a function of integrated BP and integrated RP spectro-photometric measurements with tight constraints on the precision of these quantities (see Appendix B), there are parts of the CaMD that are not explored herein. For example, the faint end of the main sequence presented in fig. 9 of Gaia Collaboration et al. (2018) does not fulfill the condition on the precision in BP, so our diagrams do not include M, L, T brown dwarfs (which are fainter than  $M_G \sim 14$  mag).

There are several effects that can influence the average location of a star in the CaMD (in both axis), including interstellar extinction, stellar multiplicity, rotation, inclination of the rotation axis, and chemical composition. In this work, we do not correct for such phenomena and instead rely on the apparent magnitudes and colours measured by *Gaia*, computing ‘absolute’ magnitudes using *Gaia* parallaxes. We note that interstellar extinction and reddening can be significant at the considered distances (up to 1 kpc), in particular for objects in the Galactic plane. This leads to distortions of certain observed features, such as the long tail in the red clump extending to redder and fainter magnitudes.

The stellar variability aspects covered in the second Data Release of *Gaia* include a limited number of variability classes (Holl et al. in prep.), namely, Long Period Variables, Cepheids, RR Lyrae stars, SX Phoenicis/ $\delta$  Scuti stars,

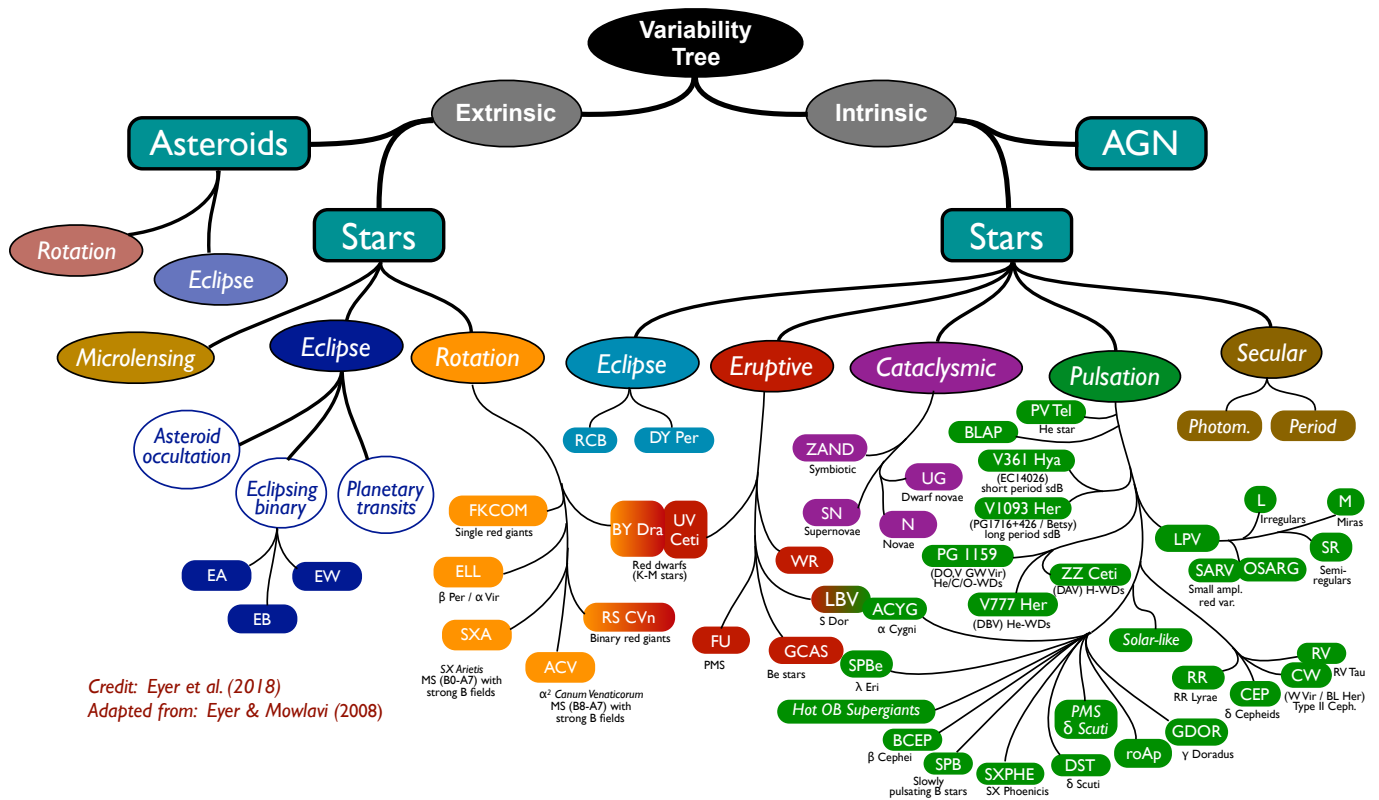


**Fig. 1.** An updated version of the variability tree presented in Eyer & Mowlavi (2008), differentiating the cause of variability phenomena: variability induced by pulsations, rotation, eruptions, eclipses, and cataclysmic events.

and rotation-modulated solar-like variability (i.e., all late-type BY Draconis stars). Short time-scale variability (within one day) was explored irrespective of the physical origin of the variability (Roelens et al. in prep.), though stars classified as eclipsing binaries were removed as planned to first appear in the third Data Release of *Gaia*. The stars presented in this section are solely based on the crossmatch with known objects in the literature. The list of variability types presented here is not meant to be comprehensive.

Figures 2–6 illustrate the locations of known variable stars from catalogues in the literature that are crossmatched with the *Gaia* data. We indicate these targets according to their known variability type published in the literature (the references are listed in Table A.1), and only the stars that satisfy the selection criteria described in Appendix B are kept. Each of these figures includes as reference the location and density (in grey scale) of all stars, irrespective of stellar variability, that satisfy the astrometric and photometric criteria of Appendix B with the additional constraint of a minimum parallax of 1 mas (i.e., within 1 kpc to the Sun). This radius seems a good compromise between a large number of stars and a limited effect of interstellar matter. Variable stars whose variability type was previously known are represented by combinations of symbols and colours. Following the structure of the variability tree in Fig. 1, we show in separate figures the CaMDs of stars whose variability is induced by dif-

ferent reasons, such as pulsations, rotation, eruptions, eclipses, and cataclysmic events.

Several caveats apply to Figs. 2–6 and should be kept in mind for their interpretation. (a) The quality of catalogues published in the literature can be rather different, in part because variability is often classified without knowledge of a parallax. To reduce the impact of misclassified objects on these figures, we select subsets of all available catalogues as reference for specific variable star classes, depending on their agreement with the expected locations in the CaMD. In certain cases, we have excluded sources from the literature by choice of specific catalogues (Table A.1) and by using *Gaia*'s astrometry and the multi-band photometric time series data for occasional cuts in magnitude or colour. Future *Gaia* data releases will provide a more homogeneous variability classification that will rely primarily on the results of the variability processing (Holl et al. in prep.). (b) The CaMDs are not corrected for extinction, leading to increased scatter, in particular for objects residing primarily in heavily attenuated areas such as the Galactic disk and the Galactic bulge. (c) The cross-match of sources can be erroneous in the case of stars located in crowded regions or in the case of high proper motion, especially if the positions of stars in the published catalogues are not sufficiently precise or if proper motion information is not available. (d) *Gaia* represents a milestone for space astrometry and photometry. Nevertheless, some sources can be affected by issues

such as corrupt measurements so that their location in the CaMD may be incorrect (Arenou et al. 2018). However, we stress that such issues are limited to a small fraction of sources so that most known variable classes are recovered as expected. The cyclic approach of the *Gaia* data processing and analysis will allow us to correct such unexpected features in the future data releases.

### 2.1. Pulsating variable stars

Figure 2 shows the positions of different classes of pulsating variable stars based on the *Gaia* data and can be compared to its theoretical counterpart in the recent textbooks on asteroseismology (fig. 1.12 in Aerts et al. 2010) and on pulsating stars (Catelan & Smith 2015). We refer to these books for further details describing specific variability classes. Here, we only consider the following types of pulsating variable stars:

1. Long Period Variables; red giant stars that populate the reddest and brightest regions of the CaMD. They include Miras, semi-regular variables, slow irregular variables, and small amplitude red giants.
2.  $\alpha$  Cygni stars; luminous supergiant stars that pulsate in non-radial modes. They are particularly affected by interstellar extinction as they are young massive stars residing in the Galactic disc, so their position in Fig. 2 must be treated with caution.
3.  $\delta$  Scuti stars; Population-I stars of spectral types A and F with short periods ( $< 0.3$  d) that pulsate in dominantly in pressure modes, but may also reveal low-order gravity modes of low amplitude.
4. SX Phoenicis stars; Population-II high amplitude  $\delta$  Scuti stars with periods typically shorter ( $< 0.2$  d) than  $\delta$  Scuti stars.
5.  $\gamma$  Doradus stars; stars with spectral type A and F stars with period from 0.3 to 3 d that pulsate dominantly in high-order gravity modes, but may also reveal low-amplitude pressure modes.
6. RR Lyrae stars (Bailey’s type ab and c); Population-II horizontal branch stars with periods from 0.2 to 1 d that pulsate in pressure mode. C-type RR Lyrae stars are bluer than ab-type stars.
7. Slowly Pulsating B (SPB) stars; non-radial multi-periodic gravity-mode pulsators of spectral type B and with periods typically in the range from 0.5 to 5 d.
8.  $\beta$  Cephei stars; late O to early-B spectral type non-supergiant stars with dominant low-order pressure and gravity modes, featuring periods in the range from 0.1 to 0.6 d. Several of them have been found to also exhibit low-amplitude high-order gravity modes as in the SPB stars (e.g., Stankov & Handler 2005). The  $\beta$  Cephei stars are located in the Galactic disc so that their CaMD position is easily affected by interstellar extinction.
9. Classical Cepheids (prototype  $\delta$  Cephei); evolved Population-I (young intermediate-mass) stars featuring radial p-mode pulsations with periods of approximately 1 – 100 d. Cepheids can be strongly affected by interstellar extinction as they reside in the Galactic disc and can be observed at great distances.
10. Type-II Cepheids; Population-II stars pulsating in p-mode that were historically thought to be identical to classical Cepheids. Type-II Cepheids consist of three different sub-classes (separated by period) commonly referred to as BL Herculis, W Virginis and RV Tauri stars, whose evolutionary scenarios differ significantly, although the three sub-classes together define a tight period-luminosity relation.

11. PV Telescopii stars; these include the sub-classes V652 Her, V2076 Oph, and FQ Aqr (Jeffery 2008), which are rare hydrogen-deficient supergiant stars that cover a wide range of spectral types and exhibit complex light and radial velocity variations.
12. Rapidly oscillating Am and Ap stars; chemically peculiar A stars that exhibit multiperiodic non-radial pressure modes in the period range of about 5 – 20 min.
13. V361 Hydrae (or EC 14026) stars; subdwarf B stars on the extreme horizontal branch that pulsate in pressure modes with very short periods of  $\sim 1$  – 10 min.
14. V1093 Her (or PG 1716) stars; subdwarf B stars on the extreme horizontal branch that pulsate in gravity modes with periods of 1 – 4 h.
15. ZZ Ceti stars; white dwarfs featuring fast non-radial gravity-mode pulsations with periods of 0.5 – 25 min.

The CaMD of pulsating stars carries a great deal of information, much of which has shaped the understanding of stellar structure and evolution and can be found in textbooks. Briefly summarized, we notice the following particularly interesting features of Fig. 2.

- Extinction affects variability classes belonging to different populations unequally, as expected. Stars located away from the Galactic disk are much less reddened and thus clump more clearly. This effect is particularly obvious when comparing RR Lyrae stars and classical Cepheids, both of which occupy the same instability strip, and cannot be explained by the known fact that the classical instability strip becomes wider in colour at higher luminosity (e.g., see Anderson et al. 2016; Marconi et al. 2005; Bono et al. 2000, and references therein).
- Interstellar reddening blurs the boundaries between variability classes. Correcting for interstellar extinction will be crucial to delineate the borders of the instability strips in the CaMD, as well as to deduce their purity in terms of the fraction of stars that exhibit pulsations while residing in such regions.
- Practical difficulties involved in separating variable star classes in the way required to construct Fig. 2 include a) that variable stars are often subject to multiple types of variability (e.g.  $\gamma$  Doradus/ $\delta$  Scuti,  $\beta$  Cephei/SPB hybrid pulsators, pulsating stars in eclipsing binary systems, or pulsating white dwarfs that exhibit eruptions), and b) that naming conventions are often historical or purely based on light curve morphology, so that they do not account for different evolutionary scenarios (e.g., type-II Cepheids). With additional data, and a fully homogeneous variable star classification based on *Gaia* alone, such ambiguities will be resolved in the future unless they are intrinsically connected to the nature of the variability.
- We notice multiple groups of ZZ Ceti stars along the white dwarf sequence. The most prominent of these is located  $G_{BP} - G_{RP} \simeq 0$  and  $M_G \simeq 12$  as seen in Fontaine & Brassard (2008)

### 2.2. Variability due to rotation and eclipses

Figure 3 shows stars whose variability is induced by rotation. There are three primary categories: spotted stars, stars deformed by tidal interactions and objects whose variability is due to light reflected by a companion. Following the nomenclature in the literature (Table A.1), we list the following variability classes separately, although we notice occasional overlaps among the

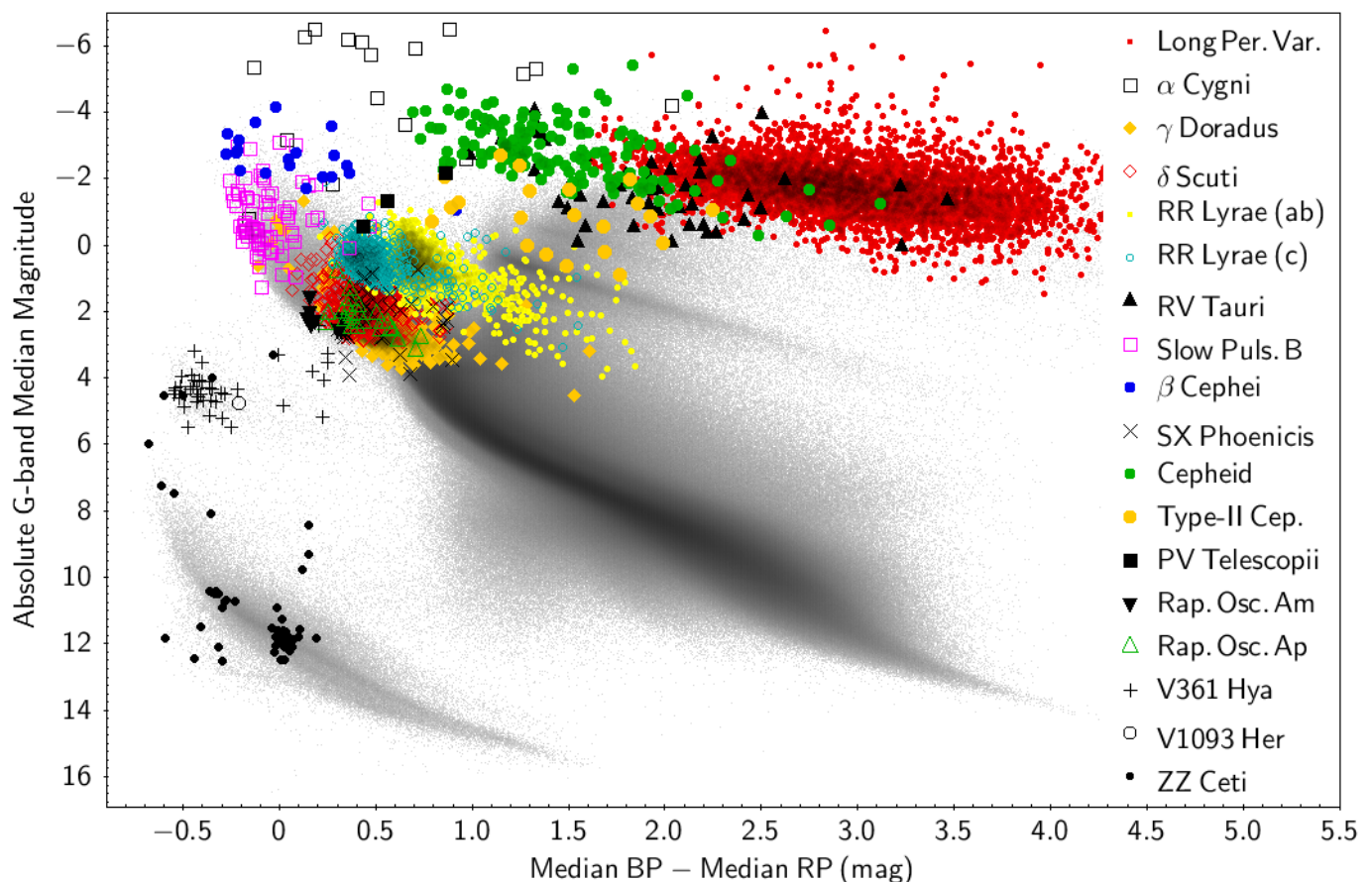


**Fig. 2.** Known pulsating variable stars retrieved from published catalogues are placed in the observational CaMD, with symbols and colours representing types as shown in the legend (see A.1 for the references from literature per type). All stars satisfy the selection criteria described in Appendix B. The background points in grey denote a reference subset of objects with a stricter constraint on parallax ( $\varpi > 1$  mas), which limits the sample size, extinction, and reddening. The effects of interstellar matter and other phenomena (see text) are not corrected for. The condition on the relative precision of  $G_{BP}$  measurements introduces artificial cuts in the distributions of low-mass main sequence stars and red (super)giants.

definitions of these variability classes. The following types are included in Fig. 3.

1.  $\alpha^2$  Canum Venaticorum stars; highly magnetic variable Bp and Ap MS stars.
2. Spotted stars; rotational modulation variability from spots.
3. BY Draconis stars; main sequence stars with late spectral types (K and M) that exhibit quasi-periodic light curves due to spots and chromospheric activity.
4. RS Canum Venaticorum stars; spotted stars whose rotation-induced variability is frequently accompanied by other phenomena, such as eclipses and flares.
5. Ellipsoidal variables; variability (without eclipses) due to orbital motion of a star distorted by a stellar companion.
6. Solar-like stars with magnetic activity. Stars of this type in Fig 3 are limited to a catalogue focused on the Pleiades, which explains a thin distribution of the main sequence. We can see a hint of the binary sequence.
7. SX Arietis stars; similar to  $\alpha^2$  Canum Venaticorum stars albeit with higher temperature. We notice that some overlap of the two distributions occurs for these two variability types.
8. Binary systems with a strong reflection component in the light curve with re-radiation of the hotter star's light from the cooler companion's surface.
9. FK Comae Berenices stars; spotted giant stars.

Figure 3 shows the following properties, among other things:

- RS Canum Venaticorum stars are significantly brighter than BY Draconis stars near the bottom of the main sequence (at cool temperatures).
- the reflection binary class is primarily present among very compact (subdwarf) stars; there is a cluster near absolute mag 4,  $G_{BP} - G_{RP} \sim -0.4$  mag.
- There seems to be a dearth of rotational spotted variables around  $G_{BP} - G_{RP} \sim 0.4$ , which corresponds with the transition region of stars with a radiative versus convective outer envelope.
- SX Arietis stars form a fairly well-defined hot temperature envelope of the most luminous  $\alpha^2$  Canum Venaticorum variables.

Figure 4 shows eclipsing binary systems as well as stars identified to host exoplanets identified by the transit method. Symbols differentiate the following sub-classes:

1. Eclipsing binaries of type EA; prototype Algol. Binaries with spherical or slightly ellipsoidal components with well-separated, nearly constant light curves in between minima. Secondary minima can be absent.
2. Eclipsing binaries of type EB; prototype  $\beta$  Lyrae. Binaries with continuously changing light curves and not clearly defined onsets or ends of eclipses. Secondary minima are always present, but can be significantly less deep than primary minima.

3. Eclipsing binaries of type EW; prototype W Ursae Majoris. The components are nearly or actually in contact and minima are virtually equally strong. Onsets and ends of minima are not well defined.
4. Stars known to exhibit exo-planetary transits from the literature.
2. U Geminorum stars; dwarf novae, in principle consisting of a white dwarf with a red dwarf companion experiencing mass transfer.
3. Z Andromedae stars; symbiotic binary stars composed of a giant and a white dwarf.

From Fig. 4, we observe the following:

- EA stars are present almost throughout the CaMD.
- We notice groups of EB stars that are overluminous compared to the white dwarf sequence. These are likely white dwarf stars with main sequence companions.
- The majority of these stars hosting exoplanets are identified by Kepler and only very few of them have detectable transits in the *Gaia* data, because of different regimes of photometric precision and time sampling.

### 2.3. Eruptive and cataclysmic variables

Figure 5 focuses on eruptive variable stars. As for the rotationally induced variables, we adopt the nomenclature from the literature (see Table A.1), which includes partially overlapping definitions. The following types are considered.

1. S Doradus stars; Luminous Blue Variables, that is, massive evolved stars that feature major and irregular photometric variations due to heavy mass loss by a radiation-driven wind.
2. R Coronae Borealis stars; carbon rich supergiants that emit obscuring material and as a consequence have drastic rapid dimming phases.
3. Wolf-Rayet (WR) stars; the almost naked helium core left over from originally very high mass evolved stars, featuring strong emission lines of hydrogen, nitrogen, carbon, or oxygen. WR stars are undergoing very fast mass loss and can be significantly dust-attenuated.
4.  $\gamma$  Cassiopeiae stars and stars with B spectral types exhibiting hydrogen emission lines, i.e. Be stars; emitting shell stars. During their ‘eruptive’ phenomena, they become brighter.
5. Flare stars; magnetically active stars that display flares. This category includes many subtypes of magnetically active stars, such as UV Ceti-type, RS CVn-type, T Tauri stars, etc.
6. UV Ceti stars; usually K-M dwarfs displaying flares.
7. T Tauri stars (classical and weak-lined); young pre-main sequence stars, either accreting strongly (classical) or showing little sign of accretion (weak-lined). Such stars show variability due to either magnetic activity (e.g., rotational modulation, flares) or accretion (quasi-periodic, episodic, or stochastic variations), aside from pulsations that may also occur in some of them.

About Fig. 5 we comment on following properties:

- The absence of eruptive variables among hot main sequence (non supergiants) is noticeable. This region is populated by pulsating stars, such as  $\gamma$  Doradus and  $\delta$  Scuti stars, cf. Fig. 2.
- Wolf Rayet stars, R Coronae Borealis stars, and S Doradus stars are among the most luminous stars in this diagram.

Figure 6 illustrates cataclysmic variables:

1. Cataclysmic variables (generic class), typically novae and dwarf novae involving a white dwarf. Many of these stars are situated between the main and white dwarf sequences.

Further information on cataclysmic variables can be found, e.g., in Warner (2003) and Hellier (2001).

We notice the following in Fig. 6:

- There is a clump of cataclysmic variables in the ZZ Ceti variability strip location near  $G \sim 12$  and  $G_{BP} - G_{RP} \sim 0.1$ .
- The most significant clump of cataclysmic variables is near  $G \sim 4$  and  $G_{BP} - G_{RP} \sim 0.1$  mag, they are probably binary systems with stars from the extreme horizontal branch and the main sequence.

### 3. Variable Object Fractions across the CaMD

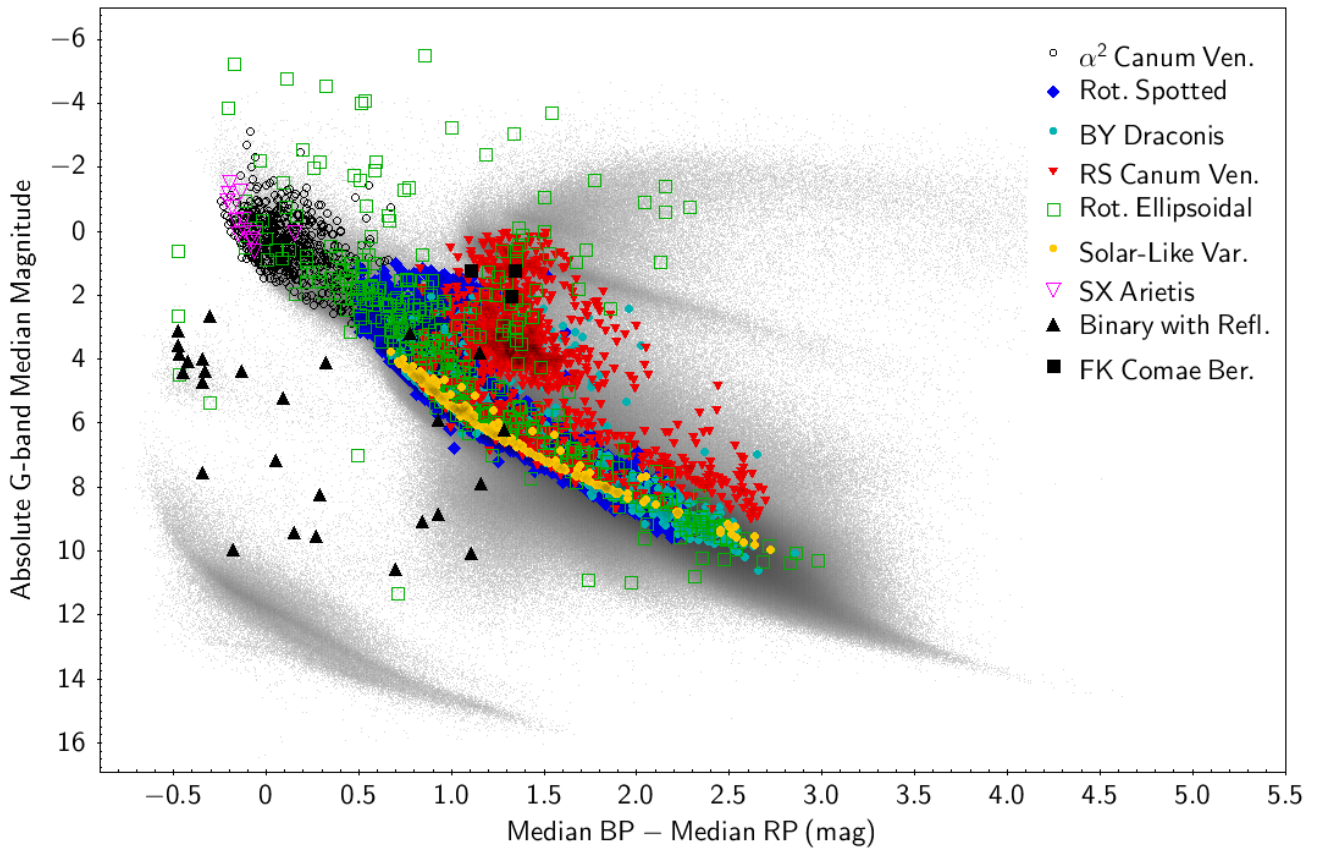
The different types of brightness variations as presented in the CaMD may strongly depend on the colour and absolute magnitude as seen in Sect. 2, because they are driven by different physical mechanisms.

Similarly, the variable object fraction – defined as the number of variable objects per colour-magnitude bin divided by the total number of objects in the same bin – is expected to depend on the location in the CaMD. The variable object fraction was previously determined based on variable objects detected using for example the *Hipparcos* time series (ESA 1997). Here we significantly expand this investigation using 13.5 million stars with heliocentric distances of up to 1 kpc that satisfy the astrometric and photometric selection criteria listed in Appendix B as well as (a) at least 20 observations in the  $G$ ,  $G_{BP}$ , and  $G_{RP}$  bands, and (b) a relative parallax error  $< 5$  per cent. In order to reduce the number of objects affected by significant extinction, stars at low Galactic latitudes (from  $-5$  to  $5$  deg) are excluded. This effectively reduces the number of disc variables such as classical Cepheids and  $\beta$  Cephei stars.

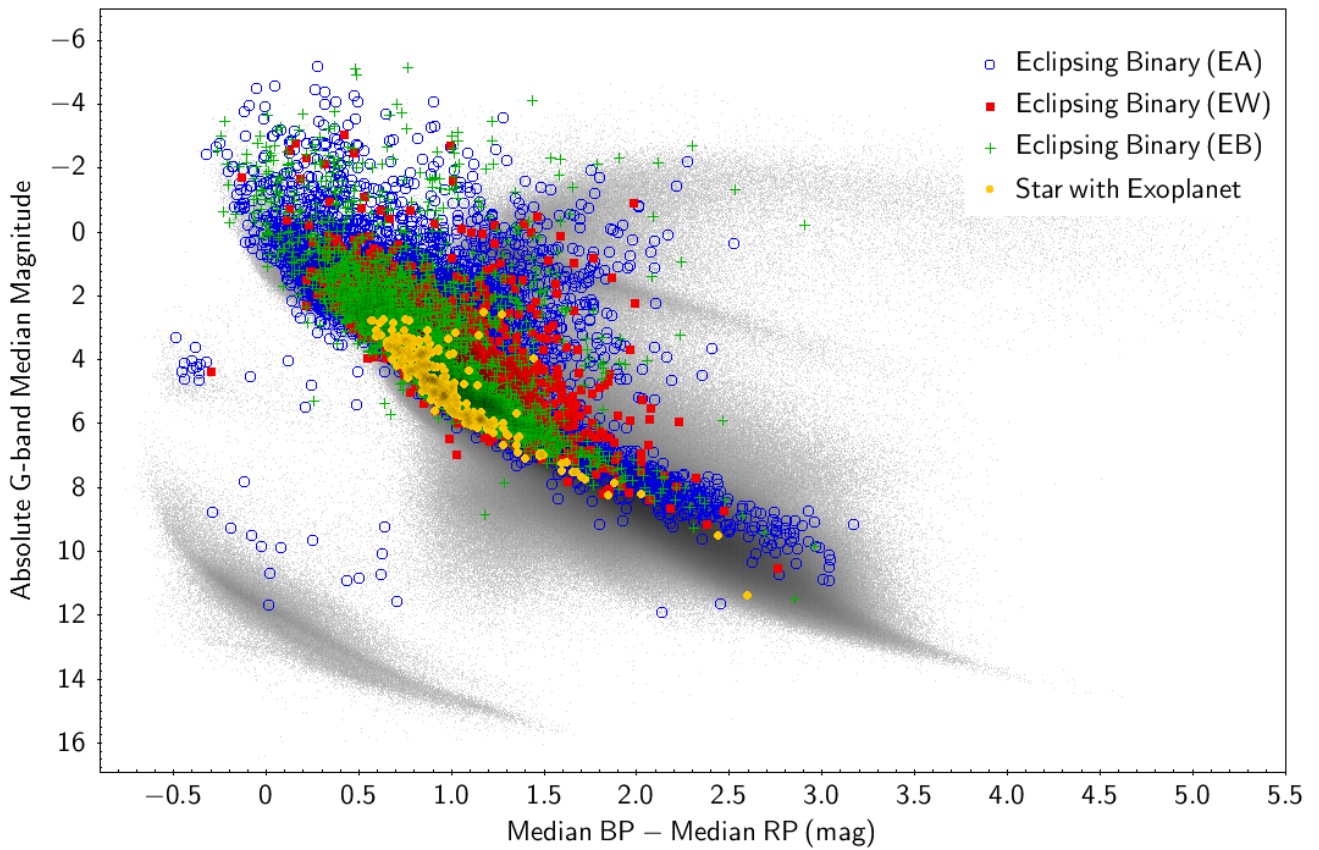
Fig. 7 illustrates this *Gaia* based high-resolution map of the variable object fraction in the CaMD at the precision level of approximately 5–10 mmag. Variability is identified in about 9 per cent of the stars based on a supervised classification of *Gaia* sources. This method depends heavily on the selection of the training set of constant and variable objects. Minor colour-coded features can be due to training-set related biases. The detection of variability further depends on the amplitude of the variables, their apparent magnitude distribution, and the instrumental precision. The accuracy of the fraction of variables is affected also by the number of sources per bin of absolute magnitude and colour, which can be as low as one in the tails of the two-dimensional source number density distribution.

Figure 7 contains many informative features, despite possible biases. Future data releases will significantly improve upon Fig. 7 by correcting for reddening and extinction and using larger number of objects with more accurate source classifications. For the time being, we remark that:

- The classical instability strip is clearly visible with variability in about 50-60 per cent of the stars (although extinction limits the precision of this estimate).
- For evolved stars, red giants, and asymptotic giant branch stars, we find that higher luminosity and redder colour implies a higher probability of variability.



**Fig. 3.** Same as Fig. 2 but for rotational-induced variability types.



**Fig. 4.** Same as Fig. 2 but for eclipsing binaries (of types EA, EB, EW) and known host-stars exhibiting exoplanet transits. As expected, eclipsing binaries can be anywhere in the CaMD, that explains why they are a main source of contamination for instance of pulsating stars.

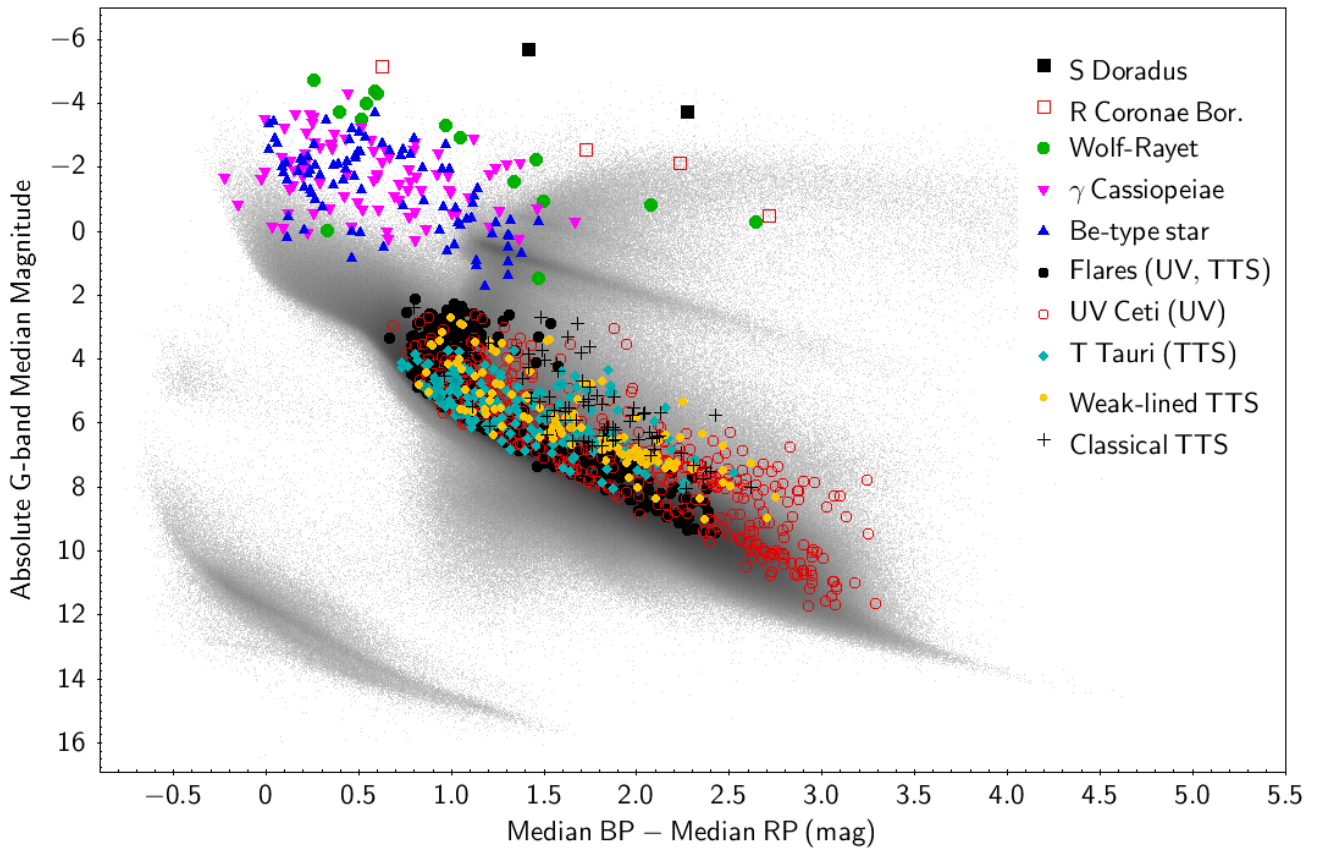


Fig. 5. Same as Fig. 2 but for eruptive variability types.

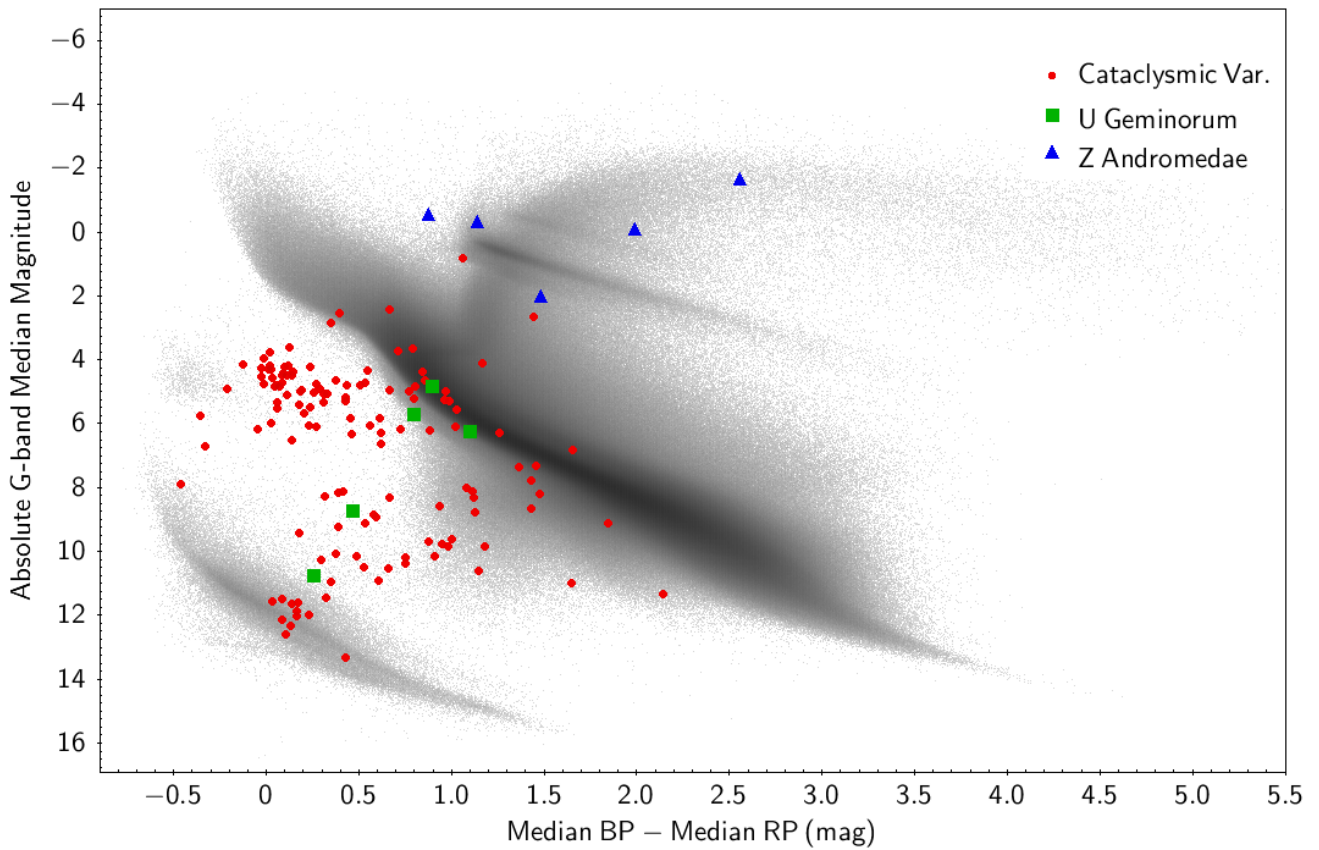
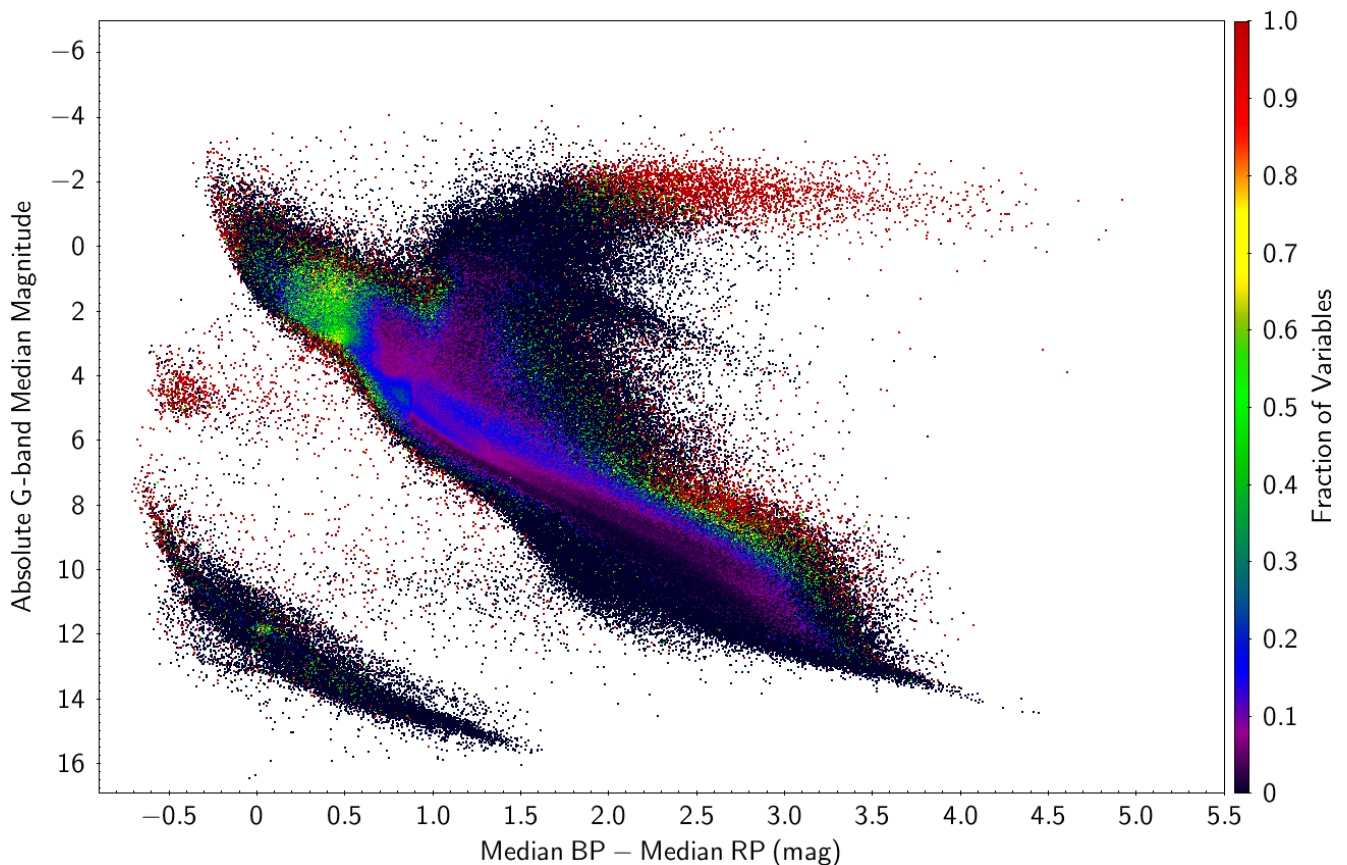


Fig. 6. Same as Fig. 2 but for cataclysmic variables and some sub-types.





**Fig. 7.** Variable object fraction across the CaMD shown as a colour scale as labeled. This figure is not based on variable objects from the literature. Instead, variability is detected directly using *Gaia* data and employing supervised classification for sources with at least 20 observations in the  $G$ ,  $G_{BP}$ , and  $G_{RP}$  bands. All objects satisfy the selection criteria described in Appendix B, but with more restrictive constraints on the parallax precision ( $\text{parallax\_over\_error} > 20$ ) and on the parallax value ( $\varpi > 1$  mas) that limits the sample (size, extinction, and reddening). In order to reduce the impact of extinction, objects at low Galactic latitudes (from  $-5$  to  $5$  deg) are excluded. About 9 per cent of the 13.5 million stars that satisfy the above mentioned criteria are variable. It is noted that some of the bins (especially the outlying ones) can contain only a few or even single sources. The condition on the relative precision of  $G_{BP}$  measurements introduces artificial cuts in the distributions of low-mass main sequence stars and red (super)giants.

- The red clump has a very low fraction of variable stars in the *Gaia* data. *Kepler* photometry of red clump stars has revealed complex variability at the  $\mu\text{mag}$  level that has been used extensively for asteroseismology, cf. Sect. 1 and references therein.
- The classical ZZ Ceti location is extremely concentrated in colour and magnitude, with variability in about half of the stars.
- Extreme horizontal branch stars show a high probability of variability.
- The hottest and most luminous main sequence stars are very frequently variable
- There is a clear gradient towards larger fractions of variables above the low-mass main sequence stars.

#### 4. Variability amplitudes across the CaMD

Figure 8 shows variability amplitudes as a function of position in the CaMD. Here, we quantify variability amplitudes using the  $G$ -band Inter-Quartile Range (IQR). Objects are selected according to the general criteria described in Appendix B, with stricter conditions on the parallax (greater than 1 mas) and its relative precision (better than 5 per cent). To prevent the false impression that faint (and very bright) sources have intrinsically higher amplitudes, we corrected for the instrumental spread of the IQR

as a function of the median  $G$  magnitude. This correction was determined using sources classified as constant in the all-sky classification (Rimoldini et al., in preparation) and subtracted in quadrature from the measured IQR. Instead of plotting individual data points in Fig. 8, we show the (colour-coded) mean of the corrected  $G$ -band IQR of sources within each square bin measuring 0.02 mag in both colour and magnitude after trimming the top and bottom 5 per cent. This binning was applied to each variability type individually, and cuts were applied to select minimum classification probabilities per type to minimize incorrect classifications. We emphasize the location of variable object classes featuring large amplitudes by plotting classes with higher IQR on top of variability classes with lower IQR.

Figure 8 contains the following stellar variability types based on the all-sky classification (Rimoldini in prep.):  $\alpha^2$  Canum Venaticorum,  $\alpha$  Cygni,  $\beta$  Cephei, cataclysmic, classical Cepheids,  $\delta$  Scuti,  $\gamma$  Cassiopeiae,  $\gamma$  Doradus, Mira, ellipsoidal, RR Lyrae of Bailey’s type ab and c, semiregular, slowly pulsating B stars, solar-like variability due to magnetic activity (flares, spots, and rotational modulation), SX Arietis, and SX Phoenicis. We did not include other classes (listed in Eyer et al. 2018) for clarity or because there were too few objects. We note that any specific selection criteria applied to the objects shown in Fig. 8 introduce biases that can highlight or diminish the prominence of certain phenomena. Nevertheless, Fig. 8 provides a first detailed illustra-

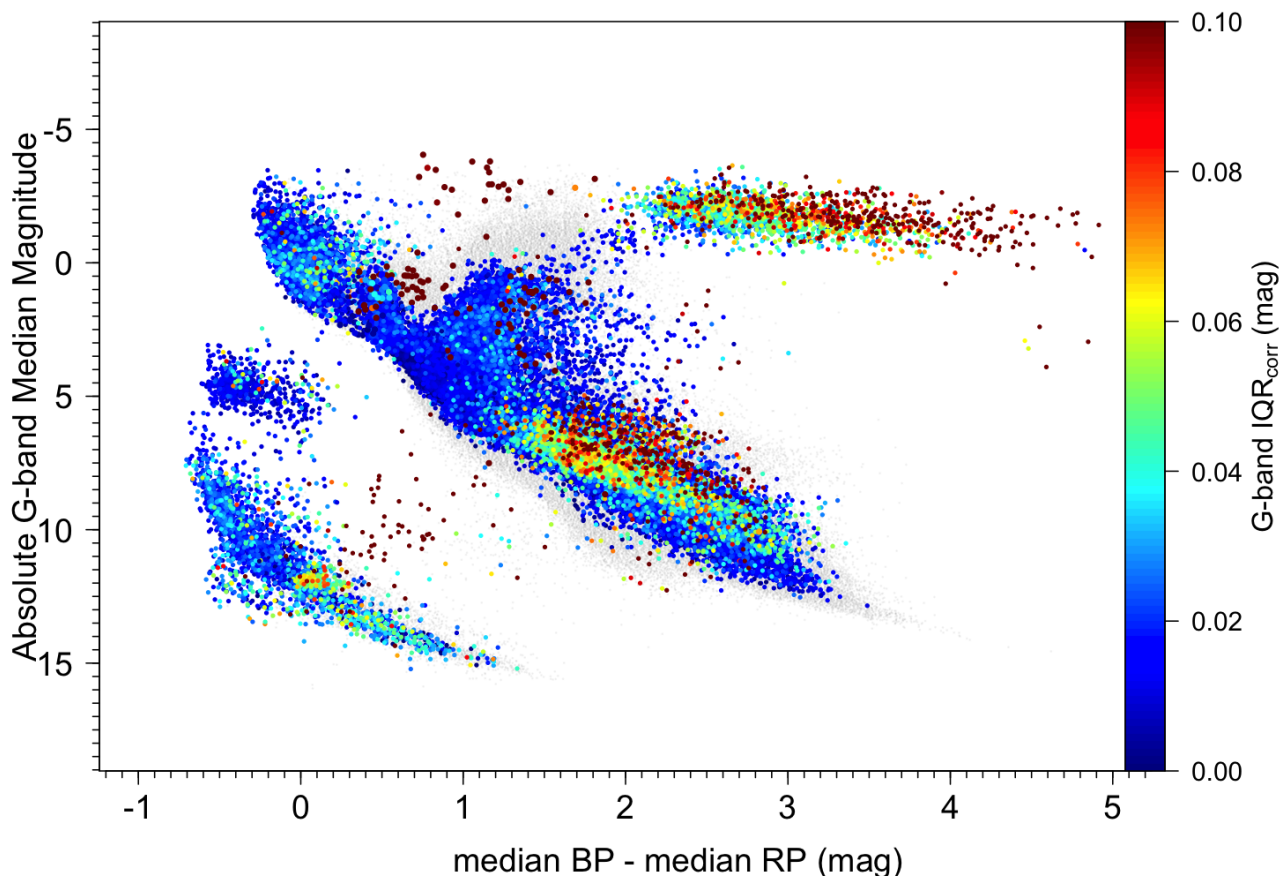


**Fig. 8.** Amplitude of variability in the CaMD, from a selection of classified variables within 1 kpc and with a relative uncertainty for the parallax of 5 per cent. The colour scale shows the corrected  $G$ -band IQR (see text) with a cut-off at 0.1 mag to emphasize the low and mid-level variability. The background points in grey represent classified constant stars. All objects satisfy the selection criteria described in Appendix B, in addition to the stricter conditions on parallax and its precision as mentioned above. The effects of interstellar extinction are not corrected for.

tion of some of the most important amplitude-related variability features across the CaMD. A number of clumps and instability regions are visible in Fig. 8, which are related to the variability classes described in Sects. 2 and 3. We notice the following trends and concentrations:

- The classical instability strip containing classical Cepheids and RR Lyrae stars is not very prominent, although some clumps (in red or cyan) are apparent.
- The instability regions linked to SPB stars and  $\beta$  Cephei stars are broad and uniform.
- Higher amplitude variations are clearly correlated with redder colours for long period variables.
- The highest amplitude (IQR > 0.1 mag) variables occur in several regions across the CaMD, including the classical instability strip, long period variables, below the red clump, above the main sequence of low-mass stars (in correspondence of the observed gradient in the fraction of variables), and between the white dwarfs sequence and the main sequence.
- Significant amplitudes of > 0.04 mag are found very frequently among the coolest white dwarfs.
- The stars between the main sequence and the white dwarfs sequence feature large variability amplitudes and extend into the clump of ZZ Ceti stars in the white dwarf sequence. This

intermediate region is populated in particular by the high-amplitude cataclysmic variables, cf. Fig. 6. A closeup view of the white dwarf sequence is shown in Fig. 9, which represents all classified variables within 200 pc, plotting each object without binning, in order to emphasize the variability of the ZZ Ceti stars.

## 5. Variability-induced motion in the CaMD

In this Section, we visualise the variability-induced motion of stars across the time-dependent CaMD using all-sky measurements made in the  $G$ ,  $G_{BP}$ , and  $G_{RP}$  passbands. *Gaia* data are uniquely suited to create this time-dependent CaMD, since the different data types – astrometric, photometric in three-band – are acquired in a quasi-simultaneous fashion at many epochs distributed over a multi-year time span. The first of such representations, although much less detailed, was first presented for individual classical Cepheids in the Milky Way (Eggen 1951) and in Galactic star clusters (Kholopov 1956; Sandage 1958). Similarly minded representations in the literature were based on data from the SDSS (Ivezic et al. 2003, mostly Galactic objects), EROS (Spano et al. 2009, LMC objects), and, very recently, the *HST* observations of M51 (Conroy et al. 2018).

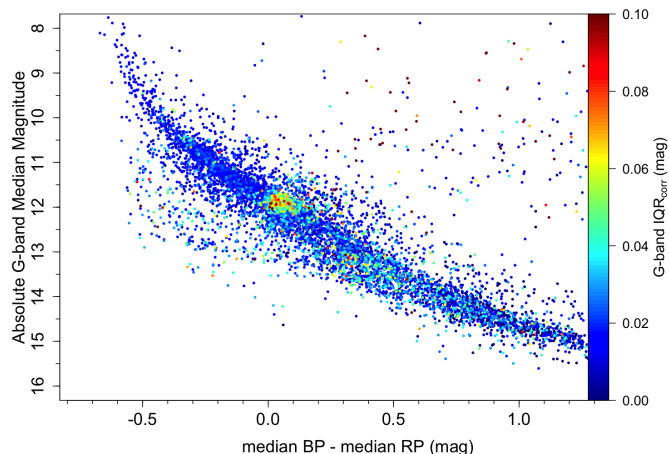


**Fig. 9.** Same as Fig. 8 but focusing on the white dwarf sequence and plotting all classified variables within 200 pc with a relative uncertainty for the parallax better than 5 per cent. A close inspection of this sequence reveals amplitudes at the level of 40 mmag in various regions.

Figure 10 illustrates the variability-induced motion of stars in the CaMD. As elsewhere in this paper, no correction for interstellar extinction is applied. Individual stars are shown by differently (arbitrarily) coloured lines that connect successive absolute  $G$  magnitudes and  $G_{BP} - G_{RP}$  measurements, i.e., the observations are ordered in time as opposed to variability phase. This choice was made to avoid uncertainties related to phase-folding the relatively sparsely-sampled light curves based on 22 or fewer months of observations and to include both periodic and non-periodic variable objects.

Figure 10 is limited to a subset of all available variable stars in order to avoid overcrowding the diagram. As a preview for future data releases, we include here the variability-induced motions of some stars whose time series and variability types are not published in DR2 (but available as online material). Figure 10 includes the following variability types defined in Sec. 2:  $\alpha^2$  Canum Venaticorum variables, B-type emission line /  $\gamma$  Cassiopeiae stars, cataclysmic variables, classical and type-II Cepheids,  $\delta$  Scuti stars, eclipsing binaries, RR Lyrae stars, long period variables, and SX Phoenicis stars. All sources shown satisfy the general criteria described in Appendix B and typically have at least 10 observations available<sup>1</sup>. We further prioritized the selection of objects featuring larger ranges of variations in the  $G$  band (with a minimum of about 0.1 mag)<sup>2</sup>. The number of sources shown per variability type ranges from a few to several tens and was selected to ensure clarity in case of high source density or overlapping variability classes in certain regions of the CaMD. In order to limit the effect of outlying values, time series data are filtered by operators as described in Holl et al. (in prep.), and the 10 per cent brightest and faintest observations in the  $G_{RP}$  band are excluded for sources with  $G_{BP} - G_{RP}$  less than 1.5 mag. Non-variable objects are shown as a grey background to provide a visual reference for the variable object locations in the CaMD. These stars satisfy the criteria described in Appendix B as well

<sup>1</sup> The minimum number of observations per source is increased to 20 in the case of long period variables, but the condition on the number of observations is removed for cataclysmic variables.

<sup>2</sup> A minimum range in the  $G$  band is not required for  $\alpha^2$  Canum Venaticorum stars and cataclysmic variables as their variability may be small in the ‘white’  $G$  band

as the stricter condition of  $\varpi > 1$  mas. Stars whose variability is caused by different physical effects exhibit different motions within the time-dependent CaMD. We briefly summarize the different motions seen in Fig.10 as follow.

1. Pulsating stars, including long period variables, Cepheids, RR Lyrae, and  $\delta$  Scuti/SX Phoenicis stars exhibit a similar behaviour. These stars are bluer when brighter in  $G$ , which illustrates that brightness variations of pulsating stars are dominated by the effect of change in temperature rather than radius. For the longest-period variables, the 22 month time span of the *Gaia* data is similar to the pulsation cycle, so that in some cases loop-like shapes are apparent. For variable stars with shorter periods (e.g., RR Lyrae stars or classical Cepheids), successive measurements in time are not generally ordered in phase, so that an overall ‘envelope’ of many cycles is revealed.
2. The motions of eclipsing binary systems in the CaMD depends on the colour difference between the two stars. The components of eclipsing systems of the EW type have similar mass (and colour), leading to a rather vertically aligned motion (parallel to the absolute magnitude axis). For eclipsing binary systems with stars of different mass (and thus colour) close to the main sequence, the deepest eclipse is usually slightly redder, since the secondary (less massive and redder) component eclipses part of the light of the primary star. The slope of the motion of eclipsing binaries in the CaMD is very different (much steeper) than the one of pulsating stars.
3. Rotationally induced variables (shown here:  $\alpha^2$  Canum Venaticorum stars) feature small amplitudes in absolute  $G$  and are rather horizontal in the CaMD. This is as expected from starspots, which have lower temperature than the surrounding and hence absorb the light at bluer frequencies to re-emit it by back warming effect at redder frequencies. Therefore, the magnitude change in a broad band like  $G$  is smaller than it would be if measured in narrow bands.
4. Eruptive stars (shown here:  $\gamma$  Cassiopeiae and Be-type stars) become redder when brighter, because of additional extinction during their eruptive phase. Hence, the slopes of their motions in the CaMD have the opposite sign with respect to the one of pulsating stars.
5. The variability of cataclysmic variables (shown here: novae) primarily features strong outbursts in the ultraviolet and blue part of the spectrum that are understood to be caused by mass transfer from donor stars in binary systems. These outbursts change very significantly the colour of the system towards bluer values.

The current version of Fig. 10 represents a first step towards a more global description of stellar variability. The motions described by the variable stars in the time-dependent CaMD provide new perspectives on the data that can be exploited as variable star classification attributes to appreciably improve the classification results. *Gaia* data will definitively help identify misclassifications and problems in published catalogues, thanks to its astrometry and the quasi-simultaneous measurements.

In future *Gaia* data releases, there will be more data points per source, making it possible to refine Fig. 10. In particular, periods can be determined with an accuracy inversely proportional to the total *Gaia* time base for periodic objects. That way, the motion in the CaMD can be represented more precisely by connecting points sorted in phase (rather than in time), leading to Lissajous-type configurations for pulsators. For sufficiently

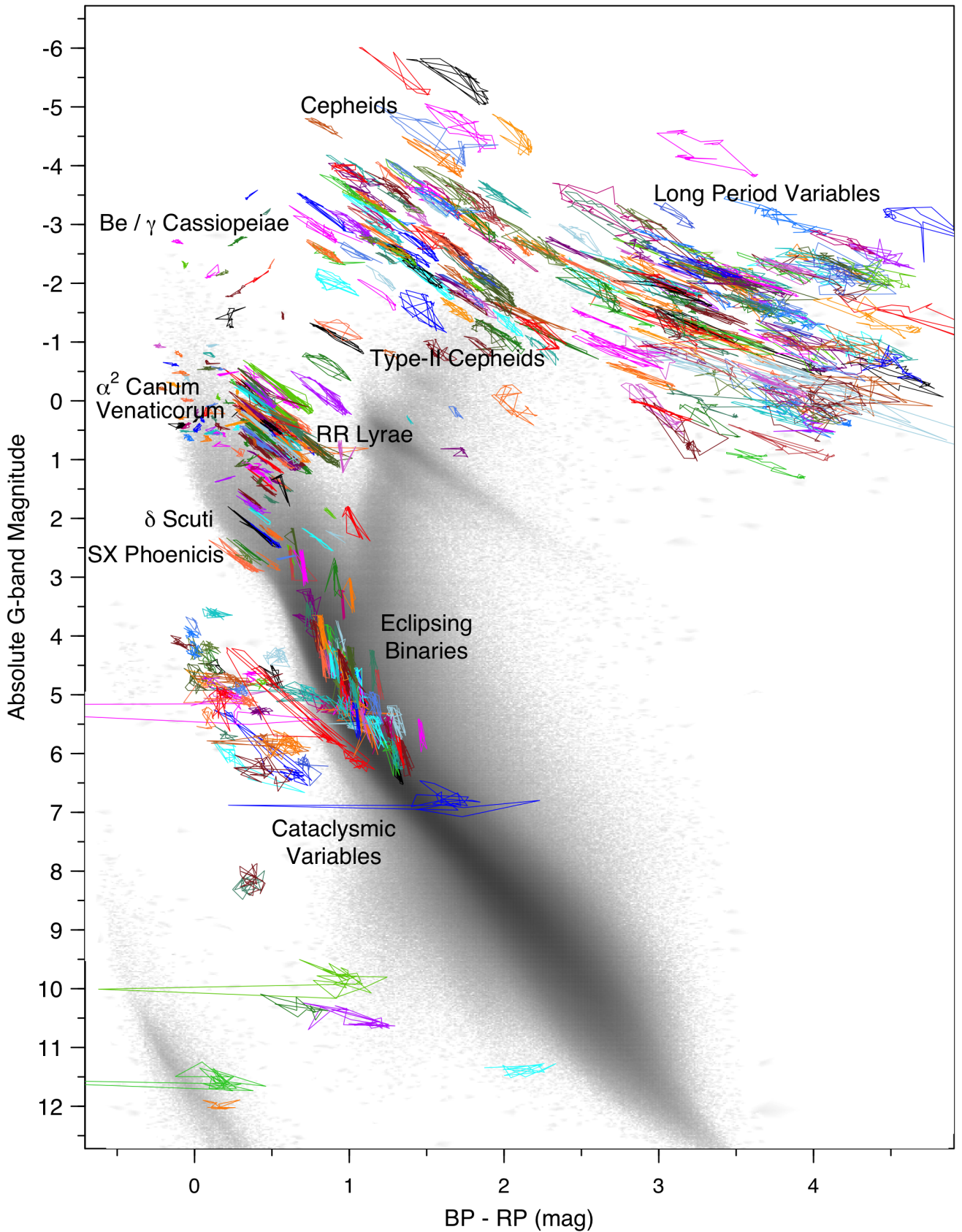


**Fig. 10.** Motions of selected variable stars in the CaMD, highlighted by segments connecting successive absolute  $G$  magnitudes and  $G_{BP} - G_{RP}$  measurements in time with the same colour for the same source. Preferential directions and amplitudes of magnitude and colour variations can be inferred as a function of variability type ( $\alpha^2$  Canum Venaticorum, Be-type and  $\gamma$  Cassiopeiae, cataclysmic, classical and type-II Cepheid,  $\delta$  Scuti and SX Phoenicis, eclipsing binary, long period, and RR Lyrae), as labelled in the Figure. For clarity of visualization, the selection of eclipsing binaries (and partially other types) was adjusted to minimize the overlap with other types. Selection criteria of all sources represented in colour or grey are the same as in Fig. 2. Additional conditions are described in the text.

bright stars, radial velocity time series will add a third and unprecedented dimension to Fig. 10.

An animated version of Fig. 10 is provided at [https://www.cosmos.esa.int/web/gaia/gaiadr2\\_cu7](https://www.cosmos.esa.int/web/gaia/gaiadr2_cu7).

## 6. Conclusions

The *Gaia* mission enables a comprehensive description of phenomena related to stellar variability. In this paper, we have focused on stellar variability across the CaMD, showcasing locations occupied by different variability types as well as variable object fractions, variability amplitudes, and variability-induced motions described by different variability classes across the CaMD.

The wealth of information related to variable stars and contained in *Gaia* DR2 is unprecedented for the Milky Way. The CaMD can provide guidance for further detailed studies, which can focus on individual regions or clumps, e.g. to investigate the purity of instability strips and how sharply such regions are truly defined or how they depend on chemical composition. Of course, additional work is required to this end, and accurately correcting for reddening and extinction will be crucial. The (time-dependent) CaMD will play an important role for improving variable star classification by providing additional attributes, such as the expected direction of variability for specific variable classes, and for illustrating stellar variability to non-expert audiences.

The CaMD of variable stars can further point out interrelations between variability phenomena that are otherwise not easily recognized and possibly identify new types of variability. Detailed follow-up observations from the ground will help correct previous misclassifications and in-depth studies of peculiar and particularly interesting objects. Thanks to the presented variable stars residing in the Milky Way, it will be possible to obtain particularly high signal-to-noise data, e.g. using high-resolution spectroscopy. Finally, the observed properties of variable stars in the CaMD, such as instability strip boundaries or period-luminosity relations, provide crucial input and constraints for models describing pulsational instability, convection, and stellar structure in general.

Future *Gaia* data releases will further surpass the variability content of this second data release<sup>3</sup>. By the end of mission, *Gaia* data are expected to comprise many tens of millions of variable celestial objects, including many additional variability types, as well as time series BP and RP spectra. Eventually, time series of radial velocities and spectra from the radial velocity spectrometer will be published for subsets of variables. Finally, the variability classification of future *Gaia* data will also make use of unsupervised clustering techniques aimed at discovering entirely new (sub-)clusters and classes of variable phenomena.

*Acknowledgements.* We would like to thank Laurent Rohrbasser for tests done on the representation of time series. This work has made use of data from the ESA space mission *Gaia*, processed by the *Gaia* Data Processing and Analysis Consortium (DPAC). Funding for the DPAC has been provided by national institutions, some of which participate in the *Gaia* Multilateral Agreement, which include, for Switzerland, the Swiss State Secretariat for Education, Research and Innovation through the ESA Prodex program, the “Mesures d’accompagnement”, the “Activités Nationales Complémentaires”, the Swiss National Science Foundation, and the Early Postdoc.Mobility fellowship; for Belgium, the BELgian federal Science Policy Office (BELSPO) through PRODEX grants; for Italy, Istituto Nazionale di Astrofisica (INAF) and the Agenzia Spaziale Italiana (ASI) through grants I/037/08/0, I/058/10/0, 2014-025-R.0, and 2014-025-R.1.2015 to INAF (PI M.G. Lattanzi); for France, the Centre National d’Etudes Spatiales (CNES). Part of this research has received

funding from the European Research Council (ERC) under the European Union’s Horizon 2020 research and innovation programme (Advanced Grant agreements N°670519: MAMSIE “Mixing and Angular Momentum transport in Massive stars”).

This research has made use of NASA’s Astrophysics Data System, the VizieR catalogue access tool, CDS, Strasbourg, France, and the International Variable Star Index (VSX) database, operated at AAVSO, Cambridge, Massachusetts, USA.

We gratefully acknowledge Mark Taylor for creating the astronomy-oriented data handling and visualization software TOPCAT (Taylor 2005).

<sup>3</sup> cf. <https://www.cosmos.esa.int/web/gaia/release>

## Appendix A: Literature per variability type

See Table A.1 for details on the references from literature regarding the objects included in Figs. 2–6 and 10.

## Appendix B: Selection criteria

Astrometric and photometric conditions are applied to all CaMDs for improved accuracy of the star locations in such diagrams. Astrometric constraints include limits on the number of visibility periods (observation groups separated from other groups by at least four days) per source used in the secondary astrometric solution (Gaia Collaboration et al. 2018), the excess astrometric noise of the source postulated to explain the scatter of residuals in the astrometric solution for that source (Gaia Collaboration et al. 2018), and the relative parallax precision (herein set to 5 but increased up to 20 in some applications):

1. `visibility_periods_used > 5`;
2. `astrometric_excess_noise < 0.5 mas`;
3. `parallax > 0 mas`;
4. `parallax_over_error > 5`.

Photometric conditions set limits for each source on the relative precisions of the mean fluxes in the  $G_{BP}$ ,  $G_{RP}$ , and  $G$  bands, as well as on the mean flux excess in the  $G_{BP}$  and  $G_{RP}$  bands with respect to the  $G$  band as a function of colour (Evans et al. 2018):

5. `phot_bp_mean_flux_error/phot_bp_mean_flux < 0.05`;
6. `phot_rp_mean_flux_error/phot_rp_mean_flux < 0.05`;
7. `phot_g_mean_flux_error/phot_g_mean_flux < 0.02`;
8. `(phot_bp_mean_flux + phot_rp_mean_flux) / {phot_g_mean_flux * [1.2 + 0.03 * (phot_bp_mean_mag - phot_rp_mean_mag)]} < 1.2`.

The ADQL query to select a sample of sources that satisfy all of the above listed criteria follows.

```
SELECT TOP 10 source_id
FROM gaiadr2.gaia_source
WHERE visibility_periods_used > 5
AND astrometric_excess_noise < 0.5
AND parallax > 0
AND parallax_over_error > 5
AND phot_bp_mean_flux_over_error > 20
AND phot_rp_mean_flux_over_error > 20
AND phot_g_mean_flux_over_error > 50
AND phot_bp_rp_excess_factor < 1.2*(1.2+0.03*
power(phot_bp_mean_mag-phot_rp_mean_mag,2))
```

## References

- Abbas, M., Grebel, E. K., Martin, N. F., et al. 2014, *AJ*, 148, 8
- Aerts, C. 2015, in *IAU Symposium*, Vol. 307, New Windows on Massive Stars, ed. G. Meynet, C. Georgy, J. Groh, & P. Stee, 154–164
- Aerts, C., Christensen-Dalsgaard, J., & Kurtz, D. W. 2010, *Asteroseismology*, Astronomy and Astrophysics Library (Springer Science+Business Media B.V.)
- Alcock, C., Allsman, R. A., Axelrod, T. S., et al. 1993, in *Astronomical Society of the Pacific Conference Series*, Vol. 43, Sky Surveys. Protostars to Protogalaxies, ed. B. T. Soifer, 291
- Alfonso-Garzón, J., Domingo, A., Mas-Hesse, J. M., & Giménez, A. 2012, *A&A*, 548, A79
- Anderson, R. I., Saio, H., Ekström, S., Georgy, C., & Meynet, G. 2016, *A&A*, 591
- Arenou, F., Luri, X., Babusiaux, C., & et al. 2018, e-print
- Auvergne, M., Bodin, P., Boisnard, L., et al. 2009, *A&A*, 506, 411
- Bedding, T. R., Mosser, B., Huber, D., et al. 2011, *Nature*, 471, 608
- Bellm, E. 2014, in *The Third Hot-wiring the Transient Universe Workshop*, ed. P. R. Wozniak, M. J. Graham, A. A. Mahabal, & R. Seaman, 27–33
- Bono, G., Castellani, V., & Marconi, M. 2000, *ApJ*, 529, 293
- Bowman, D. M. 2017, *Amplitude Modulation of Pulsation Modes in Delta Scuti Stars*, Jeremiah Horrocks Institute, University of Central Lancashire, Preston, UK. (PhD Thesis) (Springer Thesis series)
- Braga, V. F., Stetson, P. B., Bono, G., et al. 2016, *AJ*, 152, 170
- Casertano, S., Riess, A. G., Bucciarelli, B., & Lattanzi, M. G. 2017, *A&A*, 599, A67
- Catelan, M. & Smith, H. A. 2015, *Pulsating Stars* (Wiley-VCH)
- Chang, S.-W., Byun, Y.-I., & Hartman, J. D. 2015, *ApJ*, 814, 35
- Chaplin, W. J. & Miglio, A. 2013, *ARA&A*, 51, 353
- Conroy, C., Strader, J., van Dokkum, P., et al. 2018, *ArXiv e-prints*
- De Ridder, J., Molenberghs, G., Eyer, L., & Aerts, C. 2016, *A&A*, 595, L3
- Debosscher, J., Blomme, J., Aerts, C., & De Ridder, J. 2011, *A&A*, 529, A89
- Debosscher, J., Sarro, L. M., Aerts, C., et al. 2007, *A&A*, 475, 1159
- Drake, A. J., Catelan, M., Djorgovski, S. G., et al. 2013a, *ApJ*, 763, 32
- Drake, A. J., Catelan, M., Djorgovski, S. G., et al. 2013b, *ApJ*, 765, 154
- Drake, A. J., Gänsicke, B. T., Djorgovski, S. G., et al. 2014a, *MNRAS*, 441, 1186
- Drake, A. J., Graham, M. J., Djorgovski, S. G., et al. 2014b, *ApJS*, 213, 9
- EGGOS, O. J. 1951, *ApJ*, 113, 367
- EROS Collaboration, Derue, F., Afonso, C., et al. 1999, *A&A*, 351, 87
- ESA, ed. 1997, *ESA Special Publication*, Vol. 1200, The Hipparcos and Tycho catalogues. Astrometric and photometric star catalogues derived from the ESA Hipparcos Space Astrometry Mission
- Evans, D., Riello, M., De Angeli, F., & et al. 2018, e-print
- Eyer, L. & Grenon, M. 1997, in *ESA Special Publication*, Vol. 402, Hipparcos - Venice '97, ed. R. M. Bonnet, E. Høg, P. L. Bernacca, L. Emiliani, A. Blaauw, C. Turon, J. Kovalevsky, L. Lindegren, H. Hassan, M. Bouffard, B. Strim, D. Heger, M. A. C. Perryman, & L. Woltjer, 467–472
- Eyer, L., Grenon, M., Falin, J.-L., Froeschle, M., & Mignard, F. 1994, *Sol. Phys.*, 152, 91
- Eyer, L., Guy, L., & Rimoldini, L. e. a. 2018, *Gaia DR1 documentation Chapter 6: Variability*, Tech. rep., Gaia DPAC; European Space Agency
- Eyer, L. & Mowlavi, N. 2008, *Journal of Physics Conference Series*, 118, 012010
- Eyer, L., Palaversa, L., Mowlavi, N., et al. 2012, *Ap&SS*, 341, 207
- Fontaine, G. & Brassard, P. 2008, *PASP*, 120, 1043
- Gaia Collaboration, Babusiaux, C., van Leeuwen, F., Barstow, M., & et al. 2018, e-print
- Gaia Collaboration, Brown, A. G. A., Vallenari, A., et al. 2016a, *A&A*, 595, A2
- Gaia Collaboration, Clementini, G., Eyer, L., & et al. 2017, *A&A*, 605, A79
- Gaia Collaboration, Prusti, T., de Bruijne, J. H. J., et al. 2016b, *A&A*, 595, A1
- Gilliland, R. L., Brown, T. M., Christensen-Dalsgaard, J., et al. 2010, *PASP*, 122, 131
- Hartman, J. D., Bakos, G. Á., Kovács, G., & Noyes, R. W. 2010, *MNRAS*, 408, 475
- Hekker, S. & Christensen-Dalsgaard, J. 2017, *A&A Rev.*, 25, 1
- Hellier, C. 2001, *Cataclysmic Variable Stars* (Springer)
- Hermes, J. J., Kawaler, S. D., Romero, A. D., et al. 2017, *ApJ*, 841, L2
- Holl et al. in prep., *Gaia Data Release 2 – Variability Processing and Analysis Results*
- Howell, S. B., Sobek, C., Haas, M., et al. 2014, *PASP*, 126, 398
- Huber, D., Zinn, J., Bojsen-Hansen, M., et al. 2017, *ApJ*, 844, 102
- Ivezić, Ž., Lupton, R. H., Anderson, S., et al. 2003, *Mem. Soc. Astron. Italiana*, 74, 978
- Jeffery, C. S. 2008, *Information Bulletin on Variable Stars*, 5817
- Kahraman Aliçavuş, F., Niemczura, E., De Cat, P., et al. 2016, *MNRAS*, 458, 2307
- Kholopov, P. N. 1956, *Peremennye Zvezdy*, 11, 325
- Kinemuchi, K., Smith, H. A., Woźniak, P. R., McKay, T. A., & ROTSE Collaboration. 2006, *AJ*, 132, 1202
- Leavitt, H. S. 1908, *Annals of Harvard College Observatory*, 60, 87
- Leavitt, H. S. & Pickering, E. C. 1912, *Harvard College Observatory Circular*, 173, 1
- LSST Science Collaboration, Abell, P. A., Allison, J., et al. 2009, *ArXiv e-prints*
- Marconi, M., Musella, I., & Fiorentino, G. 2005, *ApJ*, 632, 590
- Mróz, P., Udalski, A., Poleski, R., et al. 2015, *Acta Astron.*, 65, 313
- Niemczura, E. 2003, *A&A*, 404, 689
- Pablo, H., Whittaker, G. N., Popowicz, A., et al. 2016, *PASP*, 128, 125001
- Palaversa, L., Ivezić, Ž., Eyer, L., et al. 2013, *AJ*, 146, 101
- Perryman, M. A. C., Lindegren, L., Kovalevsky, J., et al. 1997, *A&A*, 323
- Pigulski, A., Pojmański, G., Pilecki, B., & Szczygieł, D. M. 2009, *Acta Astron.*, 59, 33
- Rauer, H., Catala, C., Aerts, C., et al. 2014, *Experimental Astronomy*, 38, 249
- Reinhold, T. & Gizon, L. 2015, *A&A*, 583, A65
- Richards, J. W., Starr, D. L., Miller, A. A., et al. 2012, *Astrophys. J. Suppl. Series*, 203, 32
- Ricker, G. R., Winn, J. N., Vanderspek, R., et al. 2015, *Journal of Astronomical Telescopes, Instruments, and Systems*, 1, 014003

**Table A.1.** Literature references of stars as a function of variability type and the corresponding number of sources depicted in Figs. 2–6, after selections based on reliability, photometric accuracy, and astrometric parameters (Appendix B). Figure 10 includes only subsets of variability types and of sources per type.

Variability	Type	Reference	# Sources	
Pulsating	$\alpha$ Cygni	Hip97, VSX16	17	
	$\beta$ Cephei	PDC05	20	
	Cepheid	ASA09, Hip97, INT12	155	
	$\delta$ Scuti	ASA09, Hip97, JD07, Kep11b, Kep11c, SDS12	724	
	$\gamma$ Doradus	FKA16, Kep11b, Kep11c, VSX16	561	
	Long Period Variable	ASA12, Hip97, INT12, Kep11b, NSV04	5221	
	PV Telescopii	VSX16	3	
	Rapidly Oscillating Am star	VSX16	8	
	Rapidly Oscillating Ap star	VSX16	25	
	RR Lyrae, fundamental mode (RRab)	ASA09, ASA12, Cat13a, Cat13b, Cat14b, Cat15, Hip97, INT12, LIN13, NSV06, VFB16, VSX16	1676	
	RR Lyrae, first overtone (RRc)	ASA09, ASA12, Cat13b, Cat14b, Hip97, INT12, Kep11b, LIN13, MA14, VFB16, VSX16	611	
	RV Tauri	ASA12, Hip97, VSX16	48	
	Slowly Pulsating B star	IUE03, Hip97, PDC05	78	
	SX Phoenicis	ASA12, Hip97, VSX16	41	
	Type-II Cepheid	ASA12, Cat14b, Hip97, VSX16	21	
	V361 Hya (also EC 14026)	VSX16	41	
	V1093 Her (also PG 1716)	VSX16	1	
	ZZ Ceti	VSX16	61	
	Rotational	$\alpha^2$ Canum Venaticorum	Hip97, VSX16	598
		Binary with Reflection	VSX16	27
BY Draconis		VSX16	713	
Ellipsoidal		ASA12, Cat14b, Hip97, Kep11b, VSX16	398	
FK Comae Berenices		Hip97	3	
Rotating Spotted		Kep15b	16 593	
RS Canum Venaticorum		ASA12, Cat14b, Hip97, VSX16	1381	
Solar-Like Variations		HAT10	176	
SX Arietis		Hip97, VSX16	14	
Eclipsing		EA, $\beta$ Persei (Algol)	ASA09, Cat14b, Hip97, LIN13, VSX16	8123
	EB, $\beta$ Lyrae	ASA09, Cat14b, Hip97, LIN13, VSX16	3096	
	EW, W Ursae Majoris	ASA09, Hip97, VSX16	3248	
	Exoplanet	JS15	278	
Eruptive	B-type emission-line star	ASA12, VSX16	86	
	Classical T Tauri Star	VSX16	75	
	Flares (UV, BY, TTS)	Kep11a, Kep13, Kep15a, MMT15	478	
	$\gamma$ Cassiopeiae	Hip97, VSX16	84	
	R Coronae Borealis	VSX16	4	
	S Doradus	ASA12, INT12	2	
	T Tauri Star (TTS)	VSX16	173	
	UV Ceti	INT12, VSX16	425	
	Weak-lined T Tauri Star	VSX16	119	
	Wolf-Rayet	INT12, VSX16	15	
Cataclysmic	Cataclysmic Variable (generic)	Cat14a, OGL15, VSX16	132	
	U Geminorum	INT12, VSX16	4	
	Z Andromedae	INT12, VSX16	5	

**Notes.** ASA09: Pigulski et al. (2009); ASA12: Richards et al. (2012); Cat13a: Drake et al. (2013a); Cat13b: Drake et al. (2013b); Cat14a: Drake et al. (2014a); Cat14b: Drake et al. (2014b); Cat15: Torrealba et al. (2015); FKA16: Kahraman Aliçavuş et al. (2016); HAT10: Hartman et al. (2010); Hip97: ESA (1997); INT12: Alfonso-Garzón et al. (2012); IUE03: Niemczura (2003); JD07: Debosscher et al. (2007); JS15: J. Southworth, <http://www.astro.keele.ac.uk/jkt/tepcat/observables.html> (as of Aug. 2015); Kep11a: Walkowicz et al. (2011); Kep11b: Debosscher et al. (2011); Kep11c: Uytterhoeven et al. (2011); Kep13: Shibayama et al. (2013); Kep15a: Wu et al. (2015); Kep15b: Reinhold & Gizon (2015); LIN13: Palaversa et al. (2013); MA14: Abbas et al. (2014); MMT15: Chang et al. (2015); NSV04: Woźniak et al. (2004); NSV06: Kinemuchi et al. (2006); OGL15: Mróz et al. (2015); PDC05: P. De Cat, <http://www.ster.kuleuven.ac.be/~peter/Bstars/> (as of Jan. 2005); SDS12: Süveges et al. (2012); VFB16: Braga et al. (2016); VSX16: Watson et al. (2016, 2015, 2006).

- Roelens, M., Eyer, L., Mowlavi, N., et al. in prep., Gaia Data Release 2 – The Short Timescale Variability Processing and Analysis
- Sandage, A. 1958, *ApJ*, 128, 150
- Shibayama, T., Maehara, H., Notsu, S., et al. 2013, *ApJS*, 209, 5
- Spano, M., Mowlavi, N., Eyer, L., & Burki, G. 2009, in *American Institute of Physics Conference Series*, Vol. 1170, American Institute of Physics Conference Series, ed. J. A. Guzik & P. A. Bradley, 324–326
- Stankov, A. & Handler, G. 2005, *ApJS*, 158, 193
- Süveges, M., Sesar, B., Váradi, M., et al. 2012, *MNRAS*, 424, 2528
- Taylor, M. B. 2005, in *Astronomical Society of the Pacific Conference Series*, Vol. 347, *Astronomical Data Analysis Software and Systems XIV*, ed. P. Shopbell, M. Britton, & R. Ebert, 29
- Torrealba, G., Catelan, M., Drake, A. J., et al. 2015, *MNRAS*, 446, 2251
- Udalski, A., Szymański, M. K., & Szymański, G. 2015, *Acta Astron.*, 65, 1
- Uytterhoeven, K., Moya, A., Grigahcène, A., et al. 2011, *A&A*, 534, A125
- van Leeuwen, F., Evans, D. W., De Angeli, F., et al. 2017, *A&A*, 599, A32
- Walkowicz, L. M., Basri, G., Batalha, N., et al. 2011, *AJ*, 141, 50
- Warner, B. 2003, *Cataclysmic Variable Stars* (Cambridge University Press)
- Watson, C. L., Henden, A. A., & Price, A. 2006, *Society for Astronomical Sciences Annual Symposium*, 25, 47
- Watson, C. L., Henden, A. A., & Price, A. 2015, *CDS/ADC Collection of Electronic Catalogues*, 1, 2027
- Watson, C. L., Wils, P., & Ochsenbein, O. 2016, *VizieR Online Data Catalogue*, VSX Version 2016-07-04
- Woźniak, P. R., Williams, S. J., Vestrand, W. T., & Gupta, V. 2004, *AJ*, 128, 2965
- Wu, C.-J., Ip, W.-H., & Huang, L.-C. 2015, *ApJ*, 798, 92
- 
- <sup>1</sup> Department of Astronomy, University of Geneva, Ch. des Maillettes 51, CH-1290 Versoix, Switzerland
  - <sup>2</sup> Department of Astronomy, University of Geneva, Ch. d’Ecogia 16, CH-1290 Versoix, Switzerland
  - <sup>3</sup> European Southern Observatory, Karl-Schwarzschild-Str. 2, D-85748 Garching b. München, Germany
  - <sup>4</sup> SixSq, Rue du Bois-du-Lan 8, CH-1217 Geneva, Switzerland
  - <sup>5</sup> GÉPI, Observatoire de Paris, Université PSL, CNRS, Place Jules Janssen 5, F-92195 Meudon, France
  - <sup>6</sup> INAF Osservatorio di Astrofisica e Scienza dello Spazio di Bologna, Via Gobetti 93/3, I-40129 Bologna, Italy
  - <sup>7</sup> Instituut voor Sterrenkunde, KU Leuven, Celestijnenlaan 200D, 3001 Leuven, Belgium
  - <sup>8</sup> Institute of Astronomy, University of Cambridge, Madingley Road, Cambridge CB3 0HA, UK
  - <sup>9</sup> Large Synoptic Survey Telescope, 950 N. Cherry Avenue, Tucson, AZ 85719, USA
  - <sup>10</sup> Università di Catania, Dipartimento di Fisica e Astronomia, Sezione Astrofisica, Via S. Sofia 78, I-95123 Catania, Italy
  - <sup>11</sup> INAF-Osservatorio Astrofisico di Catania, Via S. Sofia 78, I-95123 Catania, Italy
  - <sup>12</sup> University of Vienna, Department of Astrophysics, Tuerkenschanzstrasse 17, A1180 Vienna, Austria
  - <sup>13</sup> Department of Geosciences, Tel Aviv University, Tel Aviv 6997801, Israel
  - <sup>14</sup> Dipartimento di Fisica e Astronomia, Università di Bologna, Via Piero Gobetti 93/2, 40129 Bologna, Italy
  - <sup>15</sup> Departamento de Astrofísica, Centro de Astrobiología (INTA-CSIC), PO Box 78, E-28691 Villanueva de la Cañada, Spain
  - <sup>16</sup> School of Physics and Astronomy, Tel Aviv University, Tel Aviv 6997801, Israel
  - <sup>17</sup> INAF-Osservatorio Astronomico di Capodimonte, Via Moiarriello 16, 80131, Napoli, Italy
  - <sup>18</sup> Dpto. Inteligencia Artificial, UNED, c/ Juan del Rosal 16, 28040 Madrid, Spain
  - <sup>19</sup> Department of Astrophysics/IMAPP, Radboud University, P.O.Box 9010, 6500 GL Nijmegen, The Netherlands
  - <sup>20</sup> Laboratoire d’astrophysique de Bordeaux, Univ. Bordeaux, CNRS, B18N, allée Geoffroy Saint-Hilaire, 33615 Pessac, France
  - <sup>21</sup> Harvard-Smithsonian Center for Astrophysics, 60 Garden Street, Cambridge, MA 02138, USA
  - <sup>22</sup> Royal Observatory of Belgium, Ringlaan 3, B-1180 Brussels, Belgium
  - <sup>23</sup> Konkoly Observatory, Research Centre for Astronomy and Earth Sciences, Hungarian Academy of Sciences, H-1121 Budapest, Konkoly Thege Miklós út 15-17, Hungary.
  - <sup>24</sup> Department of Astronomy, Eötvös Loránd University, Pázmány Péter sétány 1/a, H-1117, Budapest, Hungary
  - <sup>25</sup> Villanova University, Department of Astrophysics and Planetary Science, 800 Lancaster Ave, Villanova PA 19085, USA
  - <sup>26</sup> A. Kochoska Faculty of Mathematics and Physics, University of Ljubljana, Jadranska ulica 19, 1000 Ljubljana, Slovenia
  - <sup>27</sup> Academy of Sciences of the Czech Republic, Fricova 298, 25165 Ondřejov, Czech Republic
  - <sup>28</sup> Baja Observatory of University of Szeged, Szegedi út III/70, H-6500 Baja, Hungary.
  - <sup>29</sup> Université Côte d’Azur, Observatoire de la Côte d’Azur, CNRS, Laboratoire Lagrange, Bd de l’Observatoire, CS 34229, 06304 Nice cedex 4, France
  - <sup>30</sup> CENTRA FCUL, Campo Grande, Edif. C8, 1749-016 Lisboa, Portugal
  - <sup>31</sup> EPFL SB MATHAA STAP, MA B1 473 (Bâtiment MA), Station 8, CH-1015 Lausanne, Switzerland
  - <sup>32</sup> Warsaw University Observatory, Al. Ujazdowskie 4, 00-478 Warszawa, Poland
  - <sup>33</sup> Institute of Theoretical Physics, Faculty of Mathematics and Physics, Charles University in Prague, Czech Republic
  - <sup>34</sup> Max Planck Institute for Astronomy, Königstuhl 17, 69117 Heidelberg, Germany